Structural, Optical and Magnetic Properties of Highly Ordered Mesoporous MCr_2O_4 and $MCr_{2-x}Fe_xO_4$ (M = Co, Zn) Spinel Thin Films with Uniform 15 nm Diameter Pores and Tunable Nanocrystalline Domain Sizes

Christian Suchomski,[#] Christian Reitz,[#] Kirstin Brezesinski,[#] Célia Tavares de Sousa,[†] Marcus Rohnke,[#] Ken-ichi Iimura,[‡] Joao Pedro Esteves de Araujo,[†] and Torsten Brezesinski[#,]*

[#]Institute of Physical Chemistry, Justus-Liebig-University Giessen, Heinrich-Buff Ring 58, 35392 Giessen, Germany, [†]Departamento de Fisica, Faculdade de Ciencias, Universidade do Porto, Rua do Campo Alegre 687, 4169-007 Porto, Portugal, and [‡]Department of Advanced Interdisciplinary Science, Graduate School of Engineering, Utsunomiya University, Yoto 7-1-2, 321-8585 Utsunomiya, Japan.

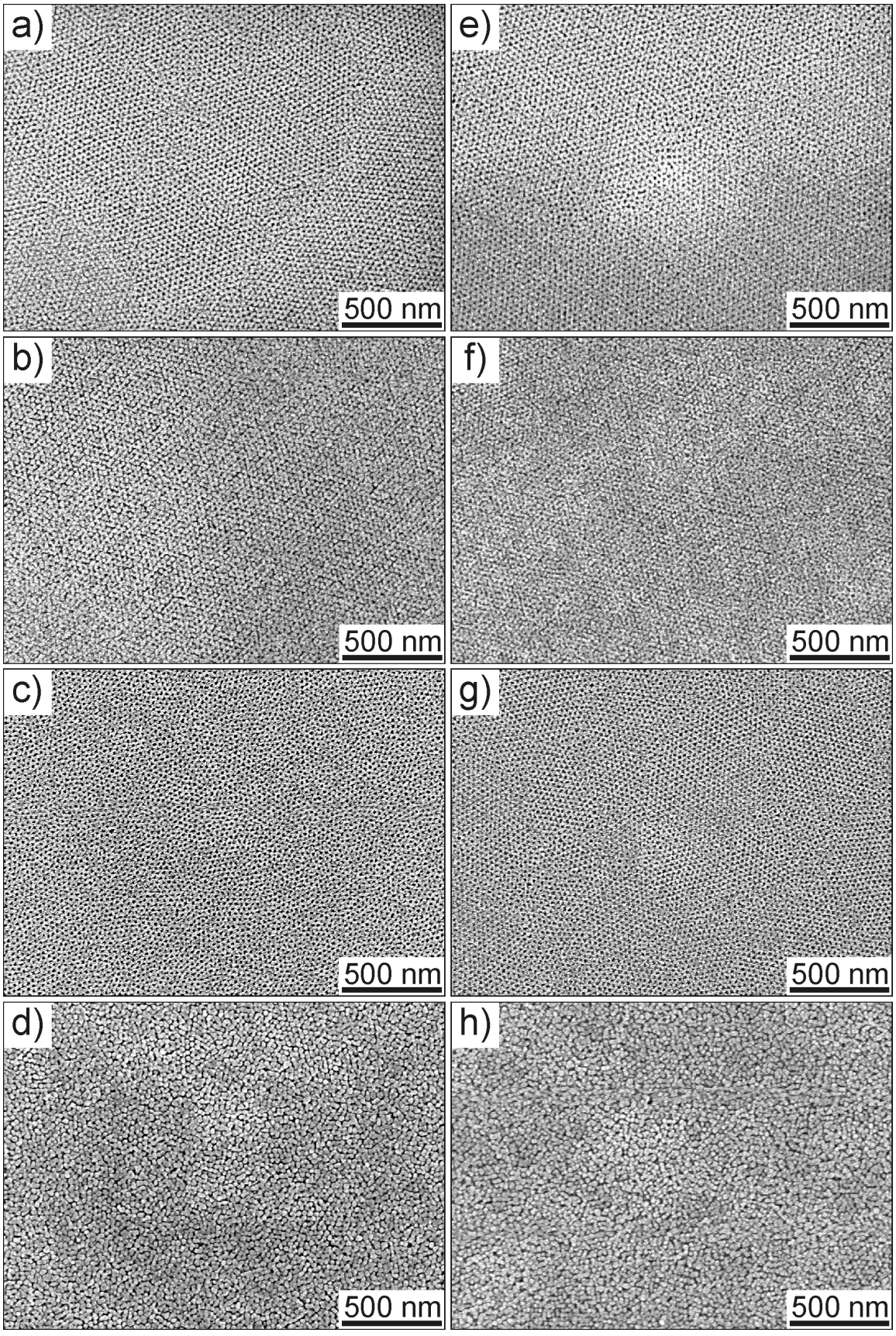
a)
500 nm
e)
500 nm
b)
500 nm
f)
500 nm
c)
500 nm
g)
500 nm
d)
500 nm
h)
500 nm

Figure S1. Morphology of KLE-templated $CoCr_2O_4$ (a,b), $CoCrFeO_4$ (c,d), $ZnCr_2O_4$ (e,f), and $ZnCrFeO_4$ (g,h) spinel thin films heated to 600 °C and 700 °C. (a,c,e,g) Low-magnification top view SEM images showing ordered cubic networks of open pores averaging 15 nm in diameter. From these data it is evident that all materials studied here are homogeneous and crack-free on the micrometer level after 600 °C. (b,d,f,h) Low-magnification top view SEM images showing that both types of solid solution thin films undergo a restructuring during high temperature treatment due to sintering effects. This restructuring is accompanied by the loss of nanoscale periodicity but produces materials with a unique morphology.

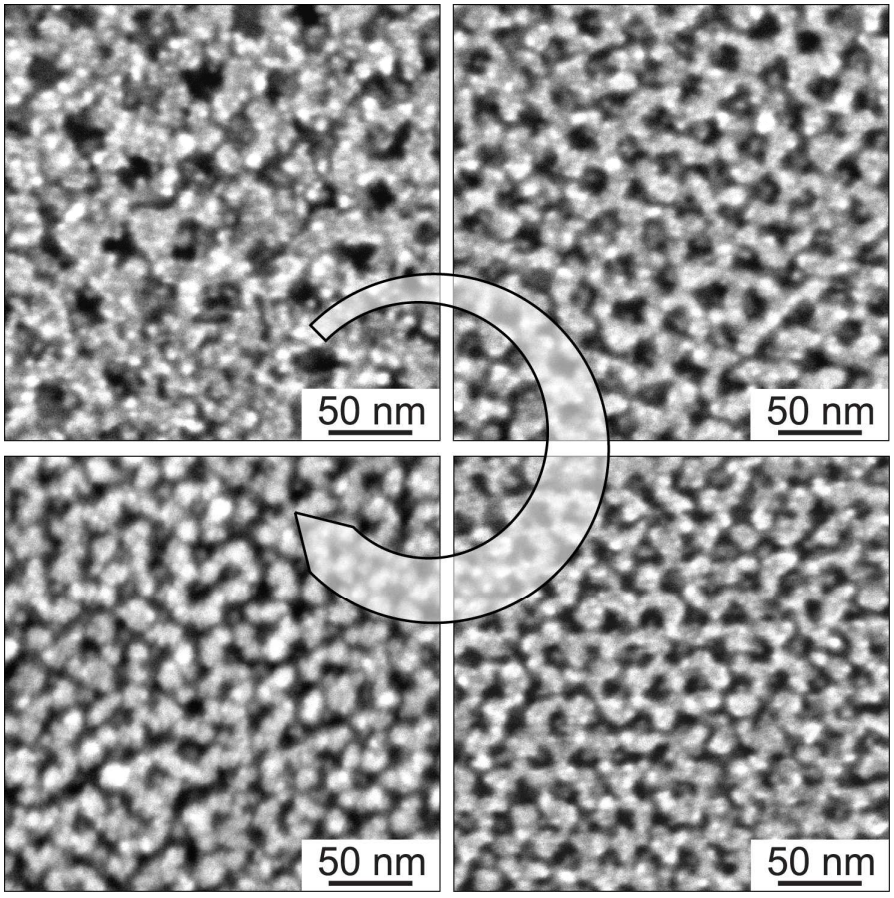

Figure S2. Top view SEM images showing the influence of the KLE mass fraction (here $m_{polymer}/m_{polymer+oxide}$) on the nanoscale structure of $CoCr_2O_4$ spinel thin films heated to 600 °C. The arrow indicates increasing mass fraction of 0.15, 0.30, 0.45, and 0.60. From this data, it can be clearly seen that a mass fraction of KLE of 0.30 gives the best results in terms of structural homogeneity (i.e., pore ordering and size) and pore wall thickness.

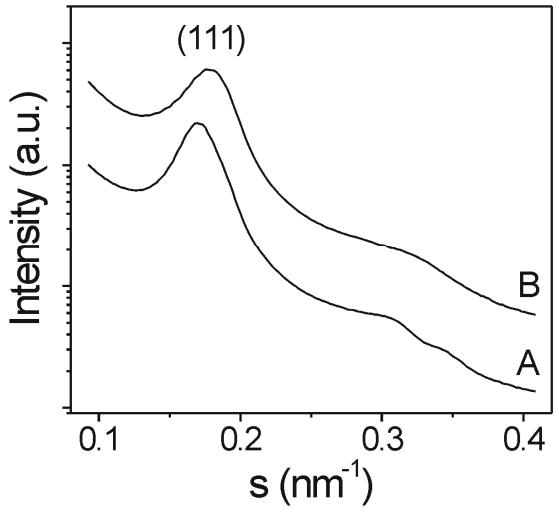

Figure S3. SAXS patterns collected in Bragg-Brentano geometry on KLE-templated $ZnCrFeO_4$ (A) and $CoCrFeO_4$ (B) thin films calcined at 250 °C for 12 h. A comparison with data in the manuscript (see Figure 4a) indicates that the solid solution thin films exhibit a lower degree of pore ordering than the bare transition metal chromites.

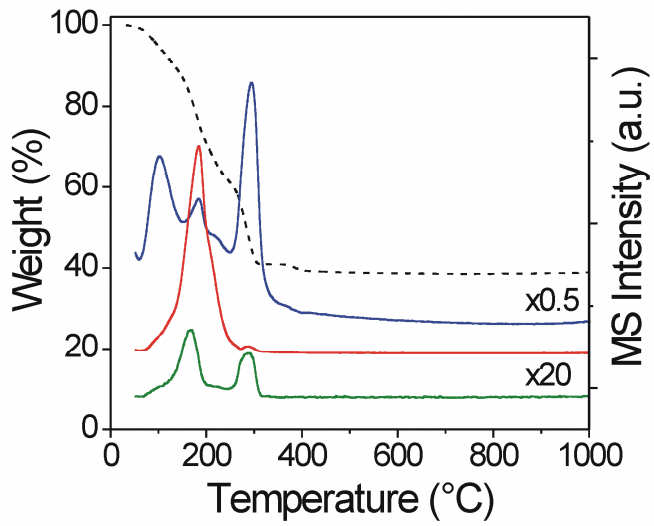

Figure S4. TGA-MS data of a homogeneous mixture of $Cr(NO_3)_3 \cdot 9H_2O$ and $Co(NO_3)_2 \cdot 6H_2O$ in the temperature range between 30 °C and 1000 °C in flowing synthetic air at a heating rate of 5 °C/min. The starting material was prepared with no polymer template but under otherwise identical conditions (see Experimental Section in the manuscript for details). The dashed line represents the TGA curve. The MS analysis shows H_2O (m/e = 18) in blue, NO (m/e = 30) in red, and NO_2 (m/e = 46) in green.

The TGA curve reveals a mass loss of ~61% by 1000 °C. TGA-MS indicates that the thermal decomposition process begins at temperatures above 60 °C and is basically completed at an annealing temperature of 300 °C (residual mass of 42%). This result is consistent with previous studies on the thermal decomposition of various hydrated metal nitrate salts. It is known that $Cr(NO_3)_3 \cdot 9H_2O$ and $Co(NO_3)_2 \cdot 6H_2O$ dissolve in their own water of crystallization below 100 °C, which is accompanied by dehydration and partial hydrolysis, i.e., formation of hydroxy nitrate species. From TGA-MS it is evident that both the nitrate and the hydroxyl groups decompose between 100 °C and 300 °C in several steps to NO/NO_2 and H_2O. Thus, during the course of

thermal treatment, several chromium and cobalt hydroxy- and oxynitrate species are formed, which ultimately convert to glassy $CoCr_2O_4$.

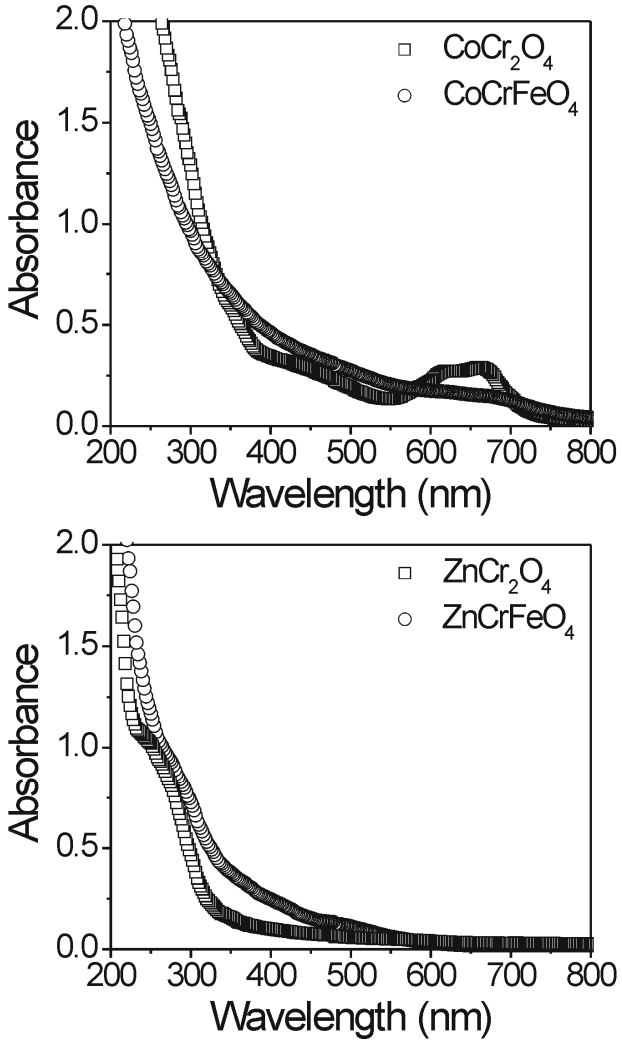

Figure S5. Absorbance spectra of KLE-templated $CoCr_2O_4$, $CoCrFeO_4$, $ZnCr_2O_4$, and $ZnCrFeO_4$ thin films on quarz substrates. The different spinel materials were heated to 650 °C prior to optical characterization.

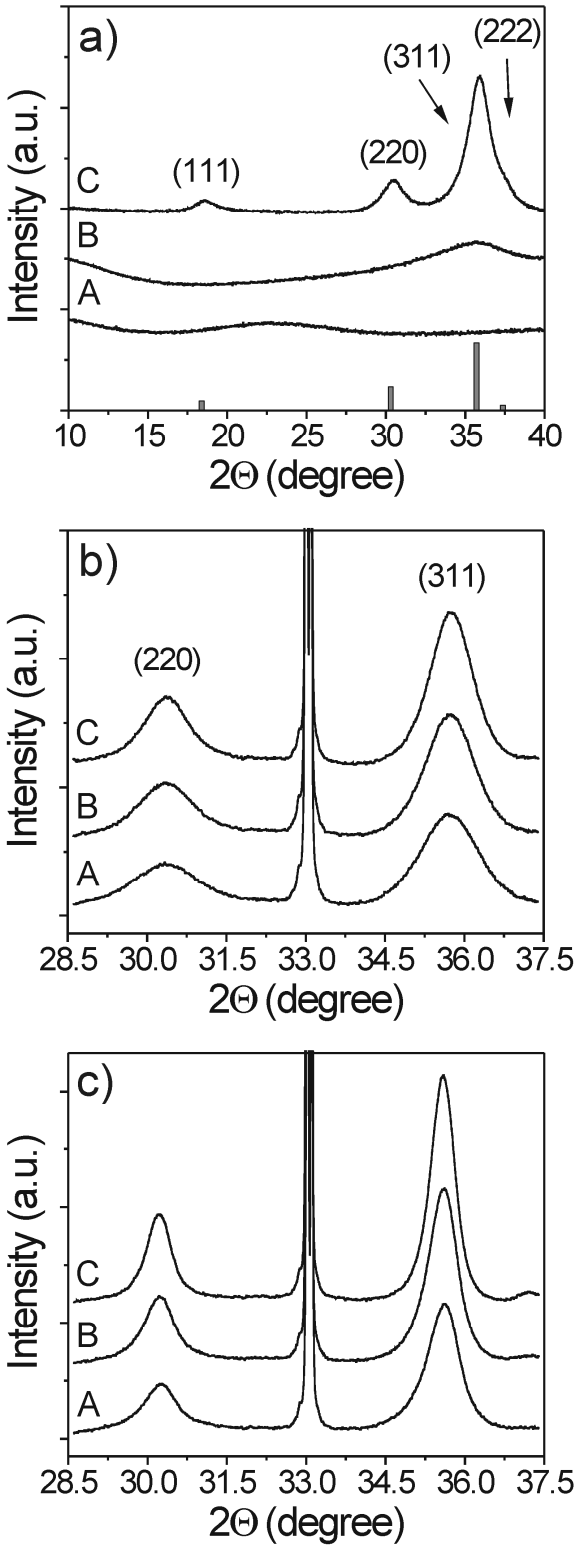
a)
(111)
(220)
(311)
(222)
C
B
A
Intensity (a.u.)
10 15 20 25 30 35 40
2Θ (degree)
b)
(220)
(311)
C
B
A
Intensity (a.u.)
28.5 30.0 31.5 33.0 34.5 36.0 37.5
2Θ (degree)
c)
C
B
A
Intensity (a.u.)
28.5 30.0 31.5 33.0 34.5 36.0 37.5
2Θ (degree)

Figure S6. WAXD patterns obtained on KLE-templated $CoCr_2O_4$ nanopowder (a) and KLE-templated $ZnCr_2O_4$ (b) and $ZnCrFeO_4$ (c) thin films. The powder material was heated to 100 °C (A), 300 °C (B), and 550 °C (C) while both thin film samples were heated to 500 °C (A), 600 °C (B), and 700 °C (C). The stick pattern in part (a) shows JCPDS (Joint Committee on Powder Diffraction Standards) reference card no. 22-1084 for cochromite.

KLE-templated $CoCr_2O_4$ in powder format heated to 100 °C shows only a broad amorphous halo centered at $2\Theta = 22.5°$. This result is characteristic of weakly cross-linked material, consisting mainly of chromium and cobalt hydroxy- and oxynitrate species, as shown in Figure S4. After thermal treatment at 300 °C, the amorphous halo is narrower and occurs at higher angles (smaller d-spacings) due to conversion to glassy $CoCr_2O_4$. The crystallization begins at approximately 550 °C and leads to phase-pure cochromite crystallites averaging 6 nm in diameter. In this regard, we note that the templated nanopowder shows a behavior very similar to that found for thin films – the KLE diblock copolymer also enables production of ordered mesoporous $CoCr_2O_4$ in powder format. The reason for the use of an amorphous $CoCr_2O_4$ nanopowder for WAXD experiments is the better signal-to-noise ratio compared to thin films due to the larger amount of material. For $ZnCr_2O_4$ and $ZnCrFeO_4$, spinel domain sizes start at 6 nm and 11 nm, respectively, and reach 9 nm and 16 nm at 700 °C.

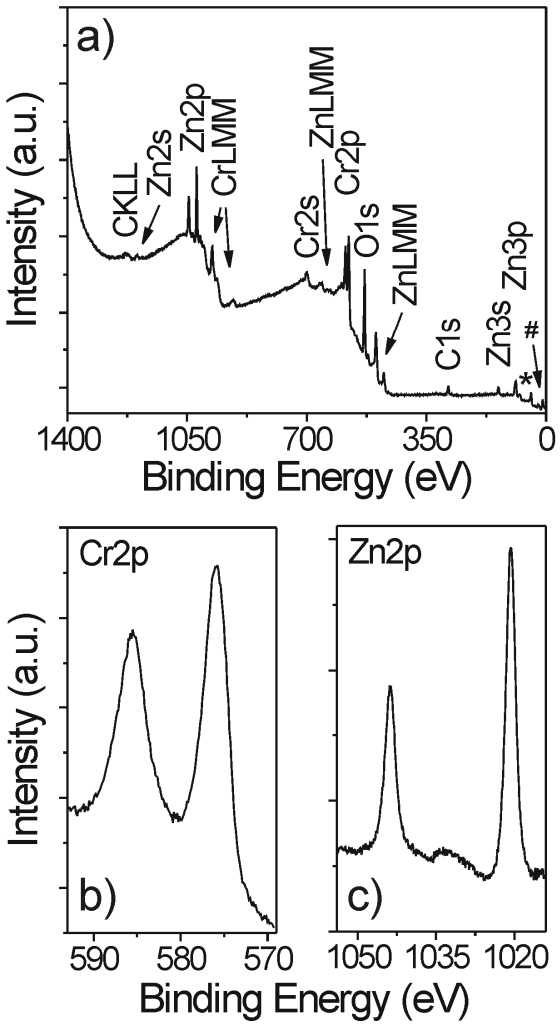

Figure S7. (a) Typical XPS survey spectrum of KLE-templated $ZnCr_2O_4$ heated to 650 °C. The Cr3s/Cr3p and O2s/Zn3d regions are indicated by (*) and (#), respectively. (b,c) High-resolution scans of the Cr2p and Zn2p core levels. Both levels consist of single doublets due to spin orbit splitting with binding energies of (585.5 ± 0.05) eV and (576.1 ± 0.05) eV for the $Cr2p_{1/2}$ and $Cr2p_{3/2}$ lines, respectively, and (1044.0 ± 0.05) eV and (1020.9 ± 0.05) eV for the $Zn2p_{1/2}$ and $Zn2p_{3/2}$ lines, respectively. Elemental analyses carried out by comparing the area of the Zn2p and Cr2p core levels reveal an atomic chromium-to-zinc ratio of 1.95 ± 0.01. The deviation from perfectly stoichiometric $ZnCr_2O_4$ is presumably due to some type of metal atom non-

stoichiometry (see also section on optical properties in the manuscript). This hypothesis is further supported by the slight asymmetry of the Cr2p lines.

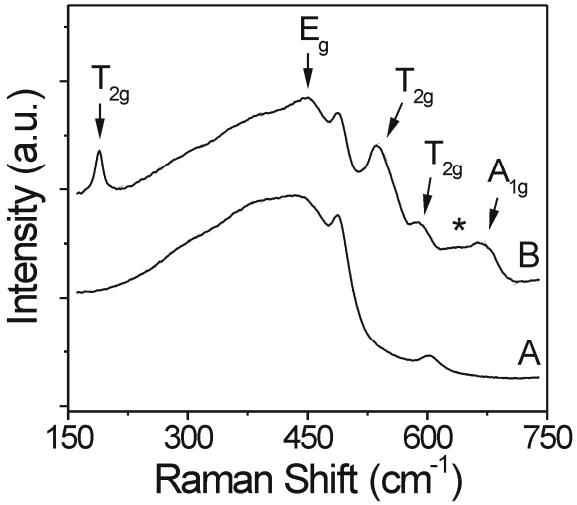

Figure S8. Raman spectra obtained on a bare quartz substrate (A) and a KLE-templated $CoCr_2O_4$ thin film on quartz. According to group theory, $CoCr_2O_4$ spinel has five Raman active phonon modes: $\Gamma = 1A_{1g} + 1E_g + 3F_{2g}$ or alternatively $3T_{2g}$. In addition to these bands, we find one more at ~640 cm^{-1} (indicated by an asterisk), which is presumably related to either some kind of cation distribution among the tetrahedral and octahedral sites or to the presence of a small fraction of Cr^{4+} on the octahedral 16(*d*) coordination sites.